



**HAL**  
open science

# MULTIFIDELITY AEROELASTIC OPTIMIZATION APPLIED TO HAR WINGS

Yoann Le Lamer, Giovanni Quaglia, Emmanuel Bénard, Joseph Morlier

► **To cite this version:**

Yoann Le Lamer, Giovanni Quaglia, Emmanuel Bénard, Joseph Morlier. MULTIFIDELITY AEROELASTIC OPTIMIZATION APPLIED TO HAR WINGS. AeroBest 2021, Jul 2021, Lisbonne, Portugal. hal-03890208

**HAL Id: hal-03890208**

**<https://hal.science/hal-03890208v1>**

Submitted on 9 Dec 2022

**HAL** is a multi-disciplinary open access archive for the deposit and dissemination of scientific research documents, whether they are published or not. The documents may come from teaching and research institutions in France or abroad, or from public or private research centers.

L'archive ouverte pluridisciplinaire **HAL**, est destinée au dépôt et à la diffusion de documents scientifiques de niveau recherche, publiés ou non, émanant des établissements d'enseignement et de recherche français ou étrangers, des laboratoires publics ou privés.



## MULTIFIDELITY AEROELASTIC OPTIMIZATION APPLIED TO HAR WINGS

Yoann Le Lamer<sup>1,2\*</sup>, Giovanni Quaglia<sup>1</sup>, Emmanuel Benard<sup>1</sup> and Joseph Morlier<sup>2</sup>

1: ISAE-Supaero  
10 Avenue Edourd Belin, 31400 Toulouse, France  
{yoann.le-lamer@isae-superaero.fr,giovanni.quaglia,  
emmanuel.benard@isae-superaero.fr}@isae-superaero.fr

2: ICA, Université de Toulouse, ISAE-SUPAERO, MINES ALBI, UPS, INSA, CNRS,  
Toulouse, France  
joseph.morlier@isae-superaero.fr

**Abstract.** *As part of a global effort toward the reduction of CO<sub>2</sub> emissions, the study of High Aspect Ratio wings is a particularly promising avenue of research. Considering this type of configuration at preliminary design stage is thus critical for optimization purposes. The use of multifidelity can help reduce computational costs by mainly running low-fidelity computations and only resorting to high-fidelity computations when necessary. The goal of this study is to develop a sufficiently accurate aero-structural model in order to fully exploit the drag reduction potential of HAR wings. The first step is to develop and apply a multifidelity approach on the CRM wing by creating a low-fidelity model. It is made sure that there is an adequate correlation between the structural modes of both high-fidelity and low-fidelity models. The so obtained low-fidelity structural model is then implemented within a in-house aeroelastic analysis and optimization framework. Afterwards, a modified version of the CRM wing with a higher aspect ratio ( $AR=13.5$ ) is considered in order to apply the same methodology with the goal to reduce significantly computational costs.*

**Keywords:** Multifidelity, High Aspect Ratio wings, Aeroelasticity, Multidisciplinary Design Optimization

## 1 INTRODUCTION

Increasing the aspect ratio of wings is one promising way to reduce CO2 emissions by limiting induced drag. In order to benefit from the full potential of these aircraft configurations, it is necessary to resort to aerostructural optimization [1]. In particular, considering computational costs is critical to achieve this goal. Indeed, in the last century, complex mathematical models have been developed in order to simulate real systems in many areas of scientific research, but the main obstacle to an intensive exploitation of such models (visualization and analysis) is the computational cost which can easily become prohibitive even for simple cases [2]. This problem is crucial in the field of aerostructural design and optimization since many simulations are required and one single CFD run may require hours of CPU time. The challenge has been tackled by creating surrogate models, sometimes also referred to as meta-models, which are an approximation of the actual system based on a number of collected samples [3]. In recent years, multifidelity (MF) has been proposed as a valuable strategy to reduce computational time. With such an approach, the results employed to train and enrich surrogate models derive from sources of different precision and are balanced in order to reduce the overall cost. These sources can be seen as black-box functions [4] and are connected to each other in an optimization environment.

In the last decade, ONERA, in a joint effort with the university ISAE-Supaero, has developed the SEGOMOE (Super Efficient Global Optimization with Mixture Of Experts) framework [5]. It is a single-fidelity, surrogate-model based, Bayesian optimization tool, able to deal with high-dimensional problems with a large number of constraints. As a further progress, [6] exploited this technique as a benchmark to demonstrate the improvements offered by the use of a multifidelity approach in terms of computational time. In this research project, a subsonic airfoil with 15 variables has been designed using MFEGO (MultiFidelity Efficient Global Optimization). This work only considers unconstrained multifidelity optimization for now. Finally, [7] produced an aeroelastic black-box function, the aerostructure package [8], also used in [9], implemented in the OpenMDAO framework [10], which optimizes the NASA CRM (Common Research Model) wing using computationally cheap aerodynamic and structural solvers.

On the one hand, regarding aerodynamics, two levels of accuracy are currently represented by a CFD and a panels code. On the other hand, the subject of this article is the development of a low-fidelity version of the structural model. It features a reduced mesh resolution, a shorter analysis time but keeps a substantial correlation with respect to the original high-fidelity model. In particular, a *MATLAB* tool has been initially designed in order to produce a FEM mesh with a level of complexity fixed by the user. Later the model properties have been assessed through different tests.

In section 2, the different theoretical arguments are discussed, along with their mathematical formulation, to support the general framework. Section 3 presents the simplifications made on the original CRM model and how the low-fidelity structural model is created. In section 4, static and dynamic behaviours are validated and the model is tested on a simple unconstrained multifidelity optimization. Then, in section 5 an aeroelastic model for the HAR uCRM-13.5 wing is presented and first aeroelastic analysis results are provided. Lastly, section 6 reports the conclusions and lists the future objectives.

## 2 THEORETICAL FRAMEWORK

### 2.1 The aerostructural problem

During the design phase of an aircraft the focus is the enhancement of multiple objective functions, namely the QoI (Quantities of Interest), such as drag or fuel consumption under mass and maximum stress constraints. In the case of steady cruise flight, the QoI are computed as result of a static aeroelastic problem. In literature, two approaches to solve it can be found, the monolithic and the partitioned. The latter is the most applied nowadays and it consists in the coupling of two different solvers for the structural and fluid problems, such as a FEM and a CFD software. The theory is reported with the notation used in [11].

$$\mathbf{y} = \mathcal{F}(\mathbf{x}), \quad \mathbf{x} = S(\mathbf{y}) \quad (1)$$

Here,  $\mathbf{x}$  and  $\mathbf{y}$  are the vectors containing the structural and aerodynamic variables, namely the nodes displacements and the fluid pressure along the airfoil.  $S$  and  $\mathcal{F}$  are the structural and fluid problems. The coupling can be expressed as:

$$\mathbf{x}^* = \arg \min_{\mathbf{x} \in \mathbb{R}^{N_s}} \|\mathcal{R}(\mathbf{x})\| \quad (2)$$

$$\text{with } \mathcal{R}(\mathbf{x}) = S \circ \mathcal{F}(\mathbf{x}) - \mathbf{x} \quad (3)$$

Once the two software required by the disciplines are chosen, they are wrapped in a framework able to process the outputs in order to be provided as inputs one to the other. Given a set of design variable, the solver iterates until a predefined convergence criterion is reached, and finally the QoI and the constraints values are extracted. Hence, the ensemble can be seen as a black-box function as shown in figure 1.

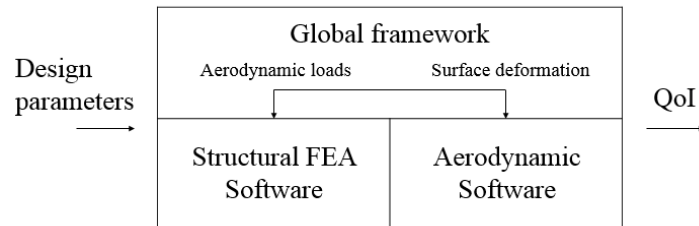


Figure 1: Black-box aeroelastic function diagram.

### 2.2 Multifidelity

The concept of multifidelity has already been introduced in the previous sections. When it is not possible to have more than few high-fidelity samples, the use of a cheaper solver allows to explore the variable design space. The large number of LF simulations permits to enrich the surrogate model and to address the optimum search. Moreover, the space of possible sources is huge. Samples used to train the model could come from experiments, software of different levels of modelling, such as CFD or panels codes in aerodynamics, a coarse and a fine mesh on the same problem or even a change in the convergence criteria

for an iterative algorithm [11]. Multifidelity is efficient if the accuracy of the optimum found is maintained while saving computational time performing less HF simulations. The main property required is the correlation between the results. The LF model must evolve in accordance with the HF one to correctly predict the behaviour of the objective function. Furthermore, the cheap code should be one or more orders of magnitude faster, allowing consistent scaling and time saving.

The theoretical background regarding MF methods is still ambiguous. While the results in terms of computational time are generally positive, it has been proven that the use of LF data can worsen the surrogate precision [12]. [13] delve into over 100 papers which make use of a MF approach. The research compared the studies in terms of levels of fidelity, disciplines, types of solvers, and data of correlation and time savings when made available. The conclusion is the absence of a clear pattern, able to determine whether or not it is convenient an MF implementation, and the lack of research in this direction.

### 3 DESIGN AND ANALYSIS OF A LOW FIDELITY STRUCTURAL MODEL

#### 3.1 General framework

The focus in the current research is optimizing the NASA CRM wing in the SEGO framework enhanced by the use of multifidelity. First of all, the programming language of the SEGO optimization algorithm is python and, in this sense, the adoption of the OpenMDAO library results extremely useful. OpenMDAO is an open-source computing platform for multidisciplinary analysis and optimization. Its structure makes it well suited for wrapping the two disciplines solvers, creating an aeroelastic black-box function. In general OpenMDAO codes are written connecting components, which can be explicit or implicit, each of them representing a part of the problem. Every component has inputs and outputs which must all be connected in the main function. Once run, the solver iterates until also the implicit parts reach convergence.

One key part of this next step in the research is the OpenMDAO package *aerostructures* [7]. The framework is used for solving static and dynamic aeroelastic analysis and optimizations. The XDSM diagram 2 presents its functioning. Each block represents a component, one can find the two main disciplines which run at their interior Panair [14], an open-source aerodynamic panels code and Nastran95 [15], used for solving the structural problem. All the other boxes have linking scopes being the interpolation and the transfer of loads and displacements between the fluid and structural mesh.

Taking advantage of this package, setting up the new optimization framework has been straightforward. The MF-EGO/MF-SEGO environment can easily encapsulate *aerostructures* and creates two versions of the main function. The first type is directly the same as before, while in the other case Panair has been substituted by a component calling the execution of the CFD software ADFlow. In this way two levels of fidelity are available. While this first version is currently being tested, one more step was needed to improve the multifidelity approach. In fact, both functions had as an input the original CRM FEM model, which is given with a high resolution mesh, weakening the possible advantages of MF. Finally, the scope of this work has been twofold. Firstly, the accuracy of the structural model has been reduced to allow faster simulations, secondly, the preserved correlation with the initial system has been analyzed. Figure 3 illustrates how the framework should resemble once this tasks have been achieved.

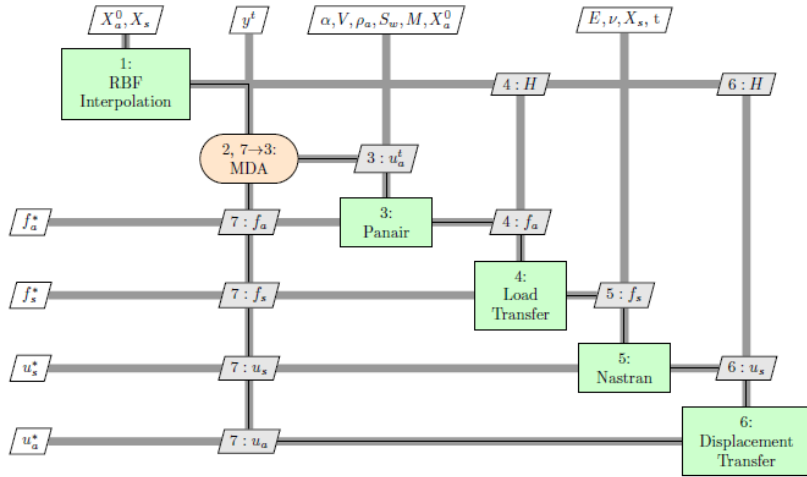


Figure 2: XDSM diagram of the static aeroelastic OpenMDAO LF solver [7].

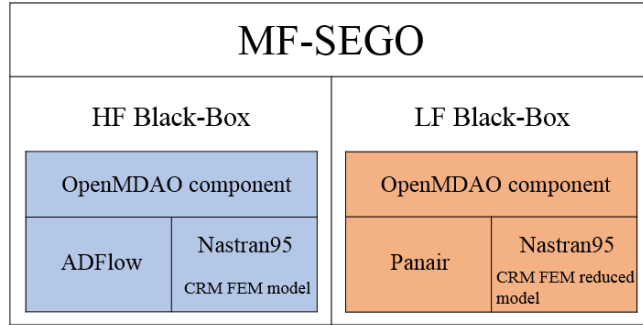


Figure 3: Diagram representing the current research framework.

### 3.2 The NASA CRM model

The Common Research Model is an attempt made by NASA to provide an experimental database for the validation of application of Computational Fluid Dynamics [16]. The related website is a repository of results from numerical and experimental analysis. In particular, some versions of different FEM models for the aircraft wing are released in Nastran language, one is drawn in figure 4. The one considered here has the following characteristics. The material is an aluminum alloy with  $\rho = 2795.67$  and  $E = 68.9$  GPa. The model consists of over 10500 nodes connected in 26600 elements. The structure is modelled as wing boxes delimited by 58 ribs closed by the upper and lower skins and with two spars at the leading and trailing edge. All this parts are explicitly represented by CQUAD4 elements depending on 12 PSHELL cards of different thickness. Moreover, ribs and skins are reinforced by stringers created with the CBAR class and with 6 different sections and principals of inertia.

### 3.3 Design phase

The first task of the project consisted in coding a routine able to receive as input the nastran *.bdf* file related to the original model and producing as outputs the reduced list of nodes and the new mesh description. As an additional objective it was planned to

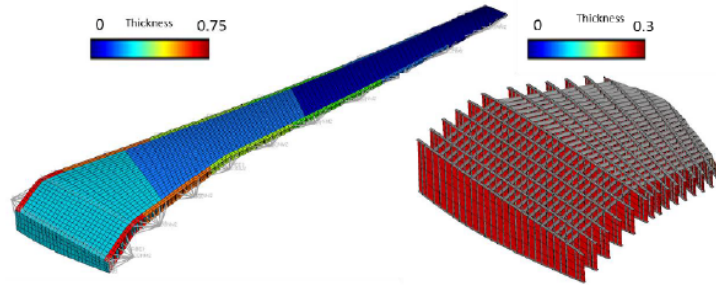


Figure 4: Illustration of the NASA CRM wing FEM model [16]

parametrise the code in order to allow choosing the desired complexity of the model. The environment used for coding the tool has been MATLAB. An early difficulty has been faced when dealing with the NASA input file. The list containing the nodes was given with no apparent order in the IDs so that it was impossible to find a mathematical law able to define their succession. As a consequence the problem has been split in writing two separate functions to order the nodes and to write the new mesh.

MainCreatePlanes.m is the first routine. One initial assumption has been made neglecting the intermediate nodes between two ribs with the outcome of having the elements representing skins and spars as long as each section. The removal of the additional rows of nodes in the cord direction diminishes the overall model flexibility with respect to the rotation around the body axis. As a result of such hypothesis the function operates with the following procedure. First, it reads a sub-list of the stringers elements inside the ribs and takes the two extreme points defining the first one. After that, it searches for a third node as the closest among the remaining and computes the 4 geometrical parameters of a plane passing through them. Finally, the node list is scanned, selecting and removing the entries whose distance from the plane is less than a fixed tolerance. The picked nodes are saved in a structure referring to a particular rib, and the process is iterated on the reduced file. As a final step, the 58 sections are sorted root to tip and the nodes belonging to each of them are locally enumerated. The result is presented in figure 5 where the initial chaotic cloud of points has been ordered.

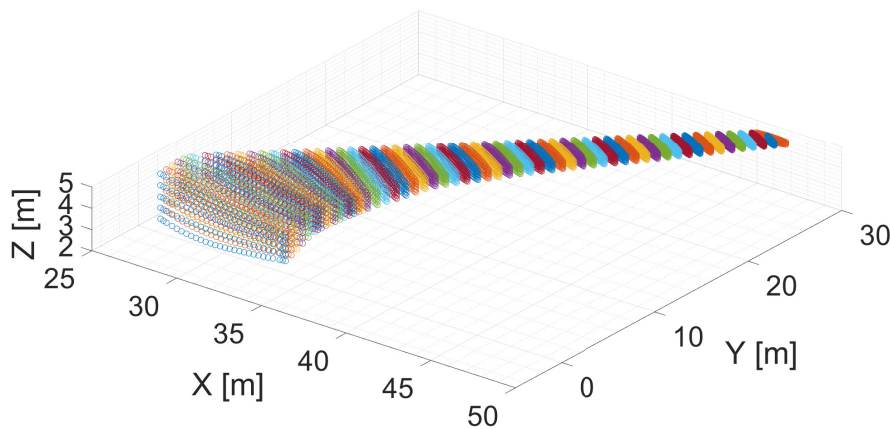


Figure 5: Matlab representation of the ordered nodes colored by rib section.

The second routine MainCreateMesh.m loads the structure containing the sorted nodes

and writes a new coarser model. At the beginning of the function two main parameters,  $L$  and  $V$ , are defined, as they set the number of points in the reduced mesh on the vertical and cord directions. One first sub-routine creates the list with the new nodes of the model. In order to accomplish this goal for each section the coordinates are transformed in a temporary reference frame so that the first two axes are in the rib plane and the third one is orthogonal to them. Then a spline interpolation is created for each row of nodes in the section, and it is evaluated in the number of points requested by  $L$  and  $V$ . The 57th rib has less nodes than the others and it is joint with the last one. Since the precise location of the intersection cannot be respected considering a coarser mesh, the function shifts all the points in the rib in order to place it as close as possible to the original. Once created, the list with the new set of nodes is taken as database by a second sub-routine which has the scope of redefining all the elements as in the starting model. The last hypothesis regards the definition of the spars. In the original CRM model they are modelled explicitly by CQUAD4 elements in a I-beam. In the spirit of reducing the complexity of the system, the flanges were substituted with simple CROD elements as they are loaded only axially in first approximation. All the elements preserve the original properties, and in particular the  $V$  vectors are reassigned to the CBAR entries looking for the closest and identically oriented stringer.

One realization of the LF structural model is presented in figure 6 for the choices of  $L = 4$  and  $V = 3$ .

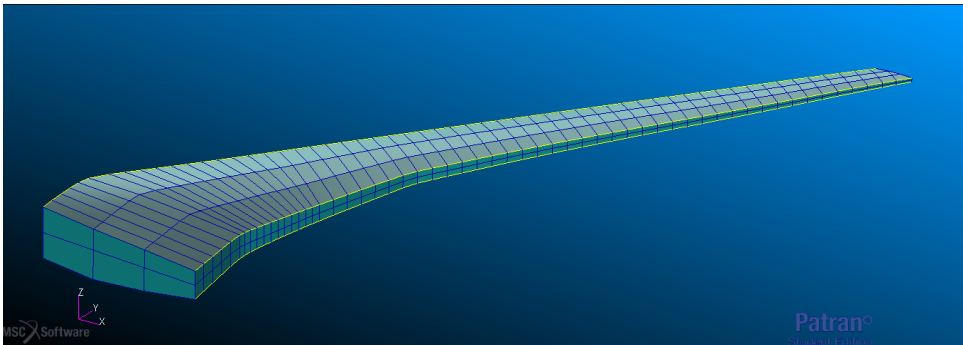


Figure 6: Low Fidelity structural model visualized in Patran for the choices of  $L = 4$  and  $V = 3$ .

The last task during the design phase consisted in adapting the python *aerostructures* package to receive the same model with different mesh definitions. In fact the structure created by the MATLAB tool would have a decreased stiffness, due to the lower number of stringers, if the geometrical and inertial properties are kept as in the HF model. The problem was overcome providing to the main function the parameters  $L$  and  $V$ , the summation on all the stringer areas and principals of inertia as well as the size of the spar flanges. A new component is then added to the OpenMDAO group and it reassigns the properties according to the actual number of bars.

## 4 MODEL VALIDATION

### 4.1 Static analysis

In a preliminary phase of the validation process, all the simulations performed were static aeroelastic problems representing the aircraft in cruise condition. After computing the



converged solution in the OpenMDAO framework, Gmsh has been used to visualize the deformation of the wing subject to the aerodynamic loads along with the Von Mises stress distribution. As an example, figure 7 compares the solution of the original model with the one obtained with the  $L = 4$  low fidelity structure. The standard geometrical values for wing surface, wing span and sweep angle were taken from the original NASA model [16], while the case parameters are reported in table 1. The QoI selected to be compared in the analysis have been the lift coefficient ( $C_l$ ) and the induced drag ( $C_{Di}$ ) computed by Panair, and the tip vertical displacement ( $\delta_{tip}$ ) and the maximum Von Mises stress ( $VM_{max}$ ) that come from the postprocessing of the Nastran95 output file.

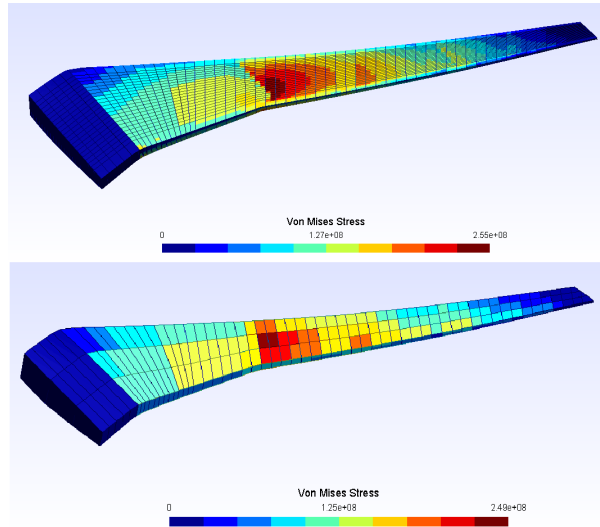


Figure 7: Gmsh visualizations of the converged solutions of the CRM wing for the HF case (up) and the  $L = 4$  LF case (down).

Table 1: Aircraft cruise input parameters.

Name	Value
Flight speed	252.16168 [m/s]
Mach number	0.85
Air density	0.380580 [kg/m <sup>3</sup> ]
Wing incidence angle	1.34 [deg]

#### 4.1.1 Mesh resolution influence

As a first step, the influence of the mesh resolution has been studied. The MATLAB tool designed was used to produce different FEM models for the parameter  $L$  varying in the interval [4-28]. The lower bound allows to have at least 2 stringers running along the wing span, while the upper bound reaches the same value of nodes in the cord direction as for the original model.

The computational cost is the major interest of MF, to this purpose, two timers, measuring the setup and run times of the OpenMDAO routine, were added to the main function . Figure 8 shows the results normalized by the values obtained running the full model. The

run time includes all the executions of Nastran95, hence it presents the greatest reduction. As expected, the line grows with a power trend due to the increasing number of elements for each node added. The key outcome is the ratio between the reference and the fastest simulation time (4), computed with  $L = 4$ . This is the maximum gain obtained and it can be called Fidelity Cost Ratio (FCR) and employed as an indicator, for example in the criterion for the next point fidelity.

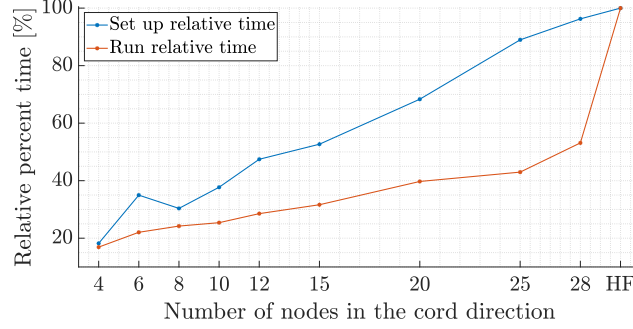


Figure 8: Setup and execution normalized timers as a function of the L parameter.

$$FCR = \frac{T_{run}^{LA}}{T_{run}^{HF}} = 16.9\% \quad (4)$$

Figure 9 shows the computed values of Cl depending on the L parameter along with the reference produced by the original model. The LF results have a general convergent trend, as the structure representation becomes more and more refined with the mesh, proving the coherent design of the model. The offset between the final values at  $L = 28$  and the HF solution is the trade-off of a MF approach. It is caused by the simplifications assumed during the design phase, namely the removal of the rib intermediate nodes, the redefinition of spars and the shifting of the next to last rib.

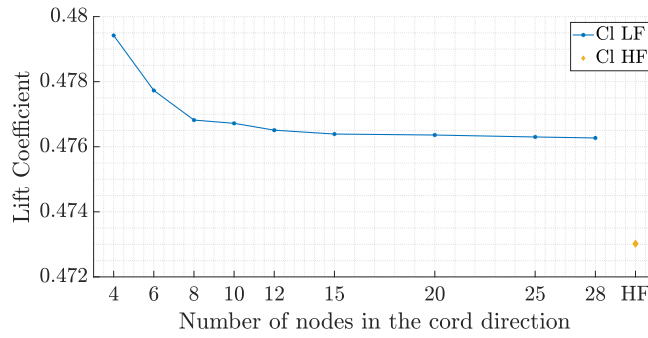


Figure 9: Lift coefficient as a function of the L parameter with reference HF value.

#### 4.1.2 Multifidelity correlation analysis

Once the MATLAB tool has been validated and the FCR computed, it was possible to focus on the correlation analysis between the LF model with  $L = 4$  and the HF original one. It is hopeful that the LF maintains the same offset found in the previous section even for other design variables inputs. For this reason maximum and minimum relative

variances must be always checked during the design space exploration. Moreover, the most important indicator is the correlation between the two fidelity, since it states if the LF can provide true information on the HF behaviour. This property has been tested in two cases, one with a random approach and one with predefined parameter steps.

In a first experiment the influence of a physical property of the structure has been analyzed. The vector containing the thickness of the 12 different PSHELL cards has been randomly modified changing its components independently inside the  $\pm 40\%$  range. 10 different realizations of the properties have been considered, the 10th being the original one. The two fidelity have been tested on each configuration. The first outcome has been the representation of the four QoI values as a function of the scalar product between the modified and original thickness vectors normalized by themselves. This index is equal to 1 when the parameters are unchanged and it decreases expressing an overall distance in the variable design space. Figure 10 presents the two fidelity results for  $\delta_{tip}$  and as well as the other graphs, it shows a perfect accordance in the results.

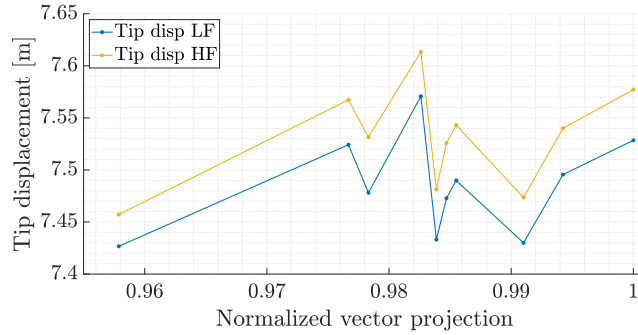


Figure 10: Tip vertical displacement as a function of the normalized projection of the shell elements thickness vectors onto the standard CRM property.

Moreover, the computation of the actual Pearson’s correlation coefficient (PCC) between the HF and LF QoI validates the trend. Table 2 reports its values along with the relative percent variances with respect to the HF results.

Table 2: Comparative indices between HF and LF for different QoI, panels thickness case.

Indices:	CI	CDi	$\delta_{tip}$	$\mathbf{VM}_{max}$
PCC	0.9995	0.9987	0.9903	0.9849
$\Delta_{max}$	1.365%	1.693%	0.704%	3.477%
$\Delta_{min}$	1.126%	0.790%	0.404%	0.219%

The second experiment has focused on the effect of two geometrical properties, the wing span ( $b$ ) and the sweep angle ( $\varphi$ ). Their standard values were  $b = 58.7629$  [m] and  $\varphi = 37.16$ , they were updated two times in both direction by a  $\Delta b = 5$  [m] and  $\Delta\varphi = 2.5$  step, resulting in 25 configuration cases. The main function was modified by the use of the *aerostructures* components able to deform the mesh according to a variation in those parameters. Figure 11 shows three realizations of the wing in the software Gmsh, the original and the two extreme cases.

In this second test the QoI has been represented on the Z axis of a 3D graph with the design variables on the XY plane. Figure 12 shows the surfaces for the  $\mathbf{VM}_{max}$  quantity.

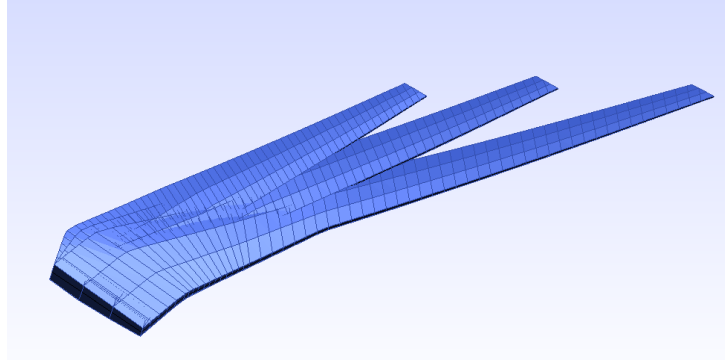


Figure 11: Gmsh visualization of the standard wing and of the two extreme configurations tested.

Once more the LF is able to correctly predict the behaviour of the HF. All the figures present a partial crossing of the surfaces for high values of the  $b$  parameter. Such long-span configuration could present some nonlinearity badly predicted by the aeroelastic function and should be object of further analysis. Finally the comparative indices, obtained from the matrices containing the QoI values, are reported in table 3.

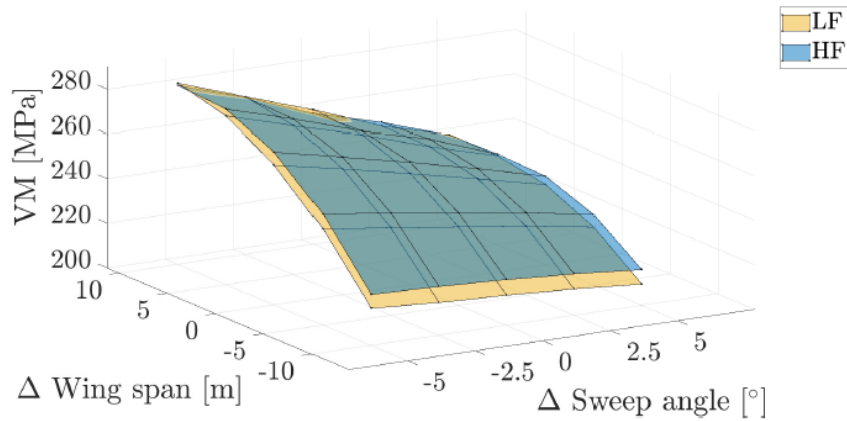


Figure 12: Maximum Von Mises stress as a function of the wing span and the sweep angle.

Table 3: Comparative indices between HF and LF for different QoI, 2 variables case.

Indices	CI	CDi	$\delta_{tip}$	$VM_{max}$
PCC	0.9998	0.9982	0.9997	0.9945
$\Delta_{max}$	1.694%	1.547%	0.884%	2.841%
$\Delta_{min}$	0.354%	0.119%	0.015%	0.118%

## 4.2 Dynamic analysis

The second phase of the validation has concerned the dynamic behaviour of the LF model. The objective has been the assessment of the correlation between the frequency response of the simplified structure and the original one. Nastran95 provides a solution for normal mode extraction even if it does not offer the same advanced options as in commercial releases. For example the standard Lanczos method is not available and thus a basic inverse

algorithm has been chosen for all the simulations. One common performance indicator for a dynamic comparison is the Modal Assurance Criterion (MAC) [17]. The Modal Assurance Criterion is a statistical indicator that is most sensitive to large differences and relatively insensitive to small differences in the mode shapes. When comparing two sets of eigenvectors in the same space, MAC indices are usually stacked in a matrix where a maximum value of 1 states full correlation, 0 being no correlation. Thus, the MAC matrix is calculated as the normalized scalar products of the two sets of vectors  $\Phi_{HF}$  and  $\Phi_{LF}$  as in (5).

$$MAC(i, j) = \frac{\|\Phi_{HF_i}^T \Phi_{LF_j}\|^2}{(\Phi_{HF_i}^T \Phi_{HF_i})(\Phi_{LF_j}^T \Phi_{LF_j})} \quad (5)$$

Mode shapes must belong to the same space, therefore the HF ones are projected, through an interpolation, onto the LF subspace. Moreover, a good practice during the comparison is to apply a mode tracking algorithm able to find the most correlated modes regardless of their extraction order. Finally, this correlation criterion takes into account only eigenvectors while frequencies must be separately compared on a relative error basis.

The first result presented in table 4 is the FCR between a 10 modes extraction for the two fidelity.

Table 4: Computational cost of modal analysis.

HF extraction	LF extraction	FCR
840.53 s	21.44 s	2.55 %

The LF model gives a sharp decrease in the computational time while the FCR value can be use as a cost index in the multifidelity optimization.

Following the static validation, the fidelity correlation has been tested on the  $b$  and  $\varphi$  design variables with the same original values and variations. Since mode shapes might shift in order from one model to the other, the code extracts 10 eigenvectors from the HF and 30 from the LF, using mode tracking to find the best matches. From each analysis it is possible to compute the MAC matrix and a table of relative errors on the first 10 modes. Figure 13 and table 5 show the results for the CRM original values of the variables. Models are proven to have great dynamic correlation, in particular no mode tracking is needed since LF frequencies are ordered and the relative error is almost zero for the first three modes.

### 4.3 Multifidelity test case application

The final part of the validation process has consisted in a simple unconstrained optimization using the MFEGO algorithm. Both the static and dynamic HF behaviours are well represented by the LF model but the latter has been chosen as analysis type. The objective function to be minimize is the inverse of the distance between the first two frequencies,  $b$  and  $\varphi$  being taken as design variables in accordance with the tests made. Thus the problem is defined as in (6).

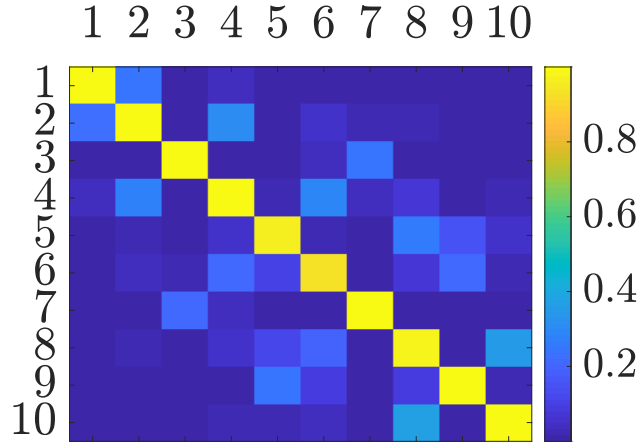

 Figure 13: MAC matrix for the original values of  $b$  and  $\varphi$ .

Table 5: Frequencies [Hz] and relative error.

HF	LF	Relative error
1.9320	1.9398	-0.400
5.7476	5.7409	0.117
7.9694	7.9275	0.525
11.650	11.402	2.126
17.672	16.227	8.172
19.002	18.413	3.102
22.289	22.067	0.992
26.817	26.038	2.906
31.016	28.620	7.725
35.742	34.826	2.561

$$\begin{aligned}
 \min_{b,\varphi} \quad & \frac{1}{f_2 - f_1} \\
 \text{for} \quad & b \in [40m, 70m] \\
 & \varphi \in [0^\circ, 30^\circ]
 \end{aligned} \tag{6}$$

The MFEGO algorithm requires two black box functions, namely the LF and HF codes for normal modes extraction, the number of points used to initially train the Co-Kriging surrogate, 7 for each fidelity, and a cost evaluation. Based on the previous section the last vector is set to  $[0.01, 1]$  and a budget of 15 is chosen. Each call of a function evaluation counts for a cost against the budget.

Figure 14 shows the initial LHS sampling of the design space. The same number of LF and HF points is chosen to train the first surrogate model.

Once the initial meta-model is obtained, the EGO algorithm successfully balances the exploration and exploitation of the design space choosing for each enrichment point the level of fidelity to be used. The final landscape is presented in figure 15 along with the location of the last point considered as optimum. Table 6 summarises the analysis results.

[3]

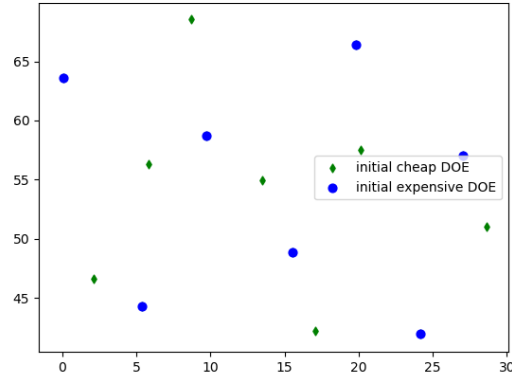


Figure 14: Initial LHS sampling in the design space.

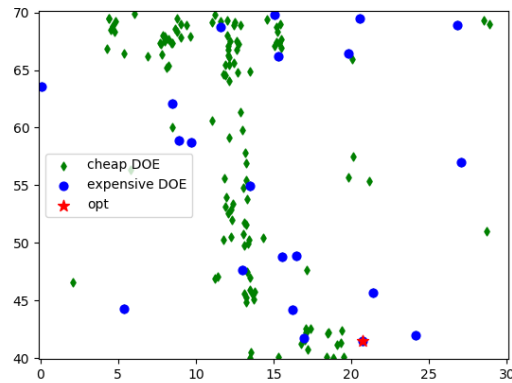


Figure 15: Design space after the optimization.

Table 6: MFEGO test results.

LF calls	127
HF call	21
Total iterations	134
$b$ solution	41.53 m
$\varphi$ solution	20.69°
Objective function	3.393786858646402e-05

The simple test performed verifies the possibility to use the new LF in a multifidelity environment. The imposed cost ratio leads the algorithm to exploit three regions using many calls of the cheap code while the HF points are fewer and better spread. Nevertheless, the number of calls to the HF model is still consistent and a further reduction of the computational cost ratio would be an interesting development. The dynamic analysis is the first step towards flutter computing in the preliminary design loop.

## 5 APPLICATION TO HAR WING

From now on, we will consider the case of an HAR wing that will be referred to uCRM-13.5, that has been developed in [18] based on on the NASA CRM by mostly increasing overall span, also referred as uCRM-9.0 in [18].

### 5.1 Design phase of HAR wing structural model

A Python script has been written to automatically creates the different sections of the wingbox and the connections between them in a BDF file format to allow analysis using MSC Nastran solver. That is done by asking the user to specify the coordinates of leading edge and trailing edge of each section. This script is parametric and thus enables one to create different wing geometries.

This script has first been tuned/developed to be able to reproduce the properties of the original NASA CRM model

Therefore, thanks to the script being parametric, it has been used to create a new model with the geometric properties of uCRM-13.5, basically with an aspect ratio increased by 50%.

As for the design of the low-fidelity model, the same procedure than the one presented in subsection 3.3 is applied to the high-fidelity HAR wing model developed previously.

### 5.2 Aeroelastic static analysis

In this subsection HF and LF aeroelastic analysis were carried for uCRM-9.0 and uCRM-13.5 models in order to determine wingtip displacement for each case. Cruise parameters used in subsection 4.3 remain unchanged. As an example, figure 16 compares wing deformations of HF and LF models for uCRM-9.0 and uCRM-13.5. Also, table 7 compares wingtip displacements for the different cases.

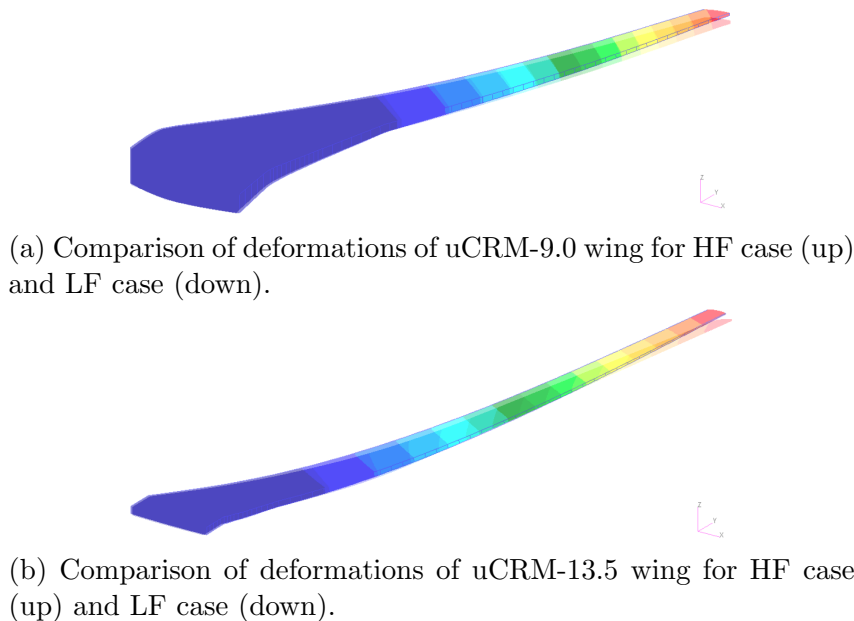


Figure 16: Comparison of deformations for uCRM-9.0 and uCRM-13.5 wings for HF and LF cases.



Table 7: Comparison of wingtip displacements between HF and LF models for uCRM-9.0 and uCRM-13.5 wings.

Model	HF model (m)	LF model (m)	Deviation (LF vs. HF in %)
uCRM-9.0	7.58	7.30	-3.69
uCRM-13.5	10.21	9.55	-6.46

As expected, higher deflections are observed for the high aspect ratio wing with regard to regular aspect ratio configuration.

The deviation of LF with regard to HF computation is satisfactory (below 5%) for uCRM-9.0 model. This deviation is higher for the high aspect ratio uCRM-13.5 model but remains reasonable (below 8%). That could be explained by the higher displacements, and the increased flexibility of HAR wing.

## 6 CONCLUSIONS

The first objectives of this research project have been achieved. First of all, the *MATLAB* tool developed in this paper is able to create a low-fidelity version of a high-fidelity wing model, whether it is the original NASA CRM model or the uCRM-13.5 model.

Static and dynamic validation results of the LF model are satisfactory in term of accuracy and correlation with regard to the HF model.

Then, we were able to develop a HF model of HAR wing uCRM-13.5, and the same simplification procedure was applied successfully. First results, show greater wingtip displacements than the original CRM as expected with reasonable deviation between HF and LF solutions.

Finally, the next step of this research project will be to accurately assess HAR wing performance while keeping reasonable computational costs for analysis and optimization. To be more specific, as higher aspect ratio wings show high rotations and displacements, structural geometrical non-linearities should be taken into account [19]. This will be done by using MSC Nastran SOL 400 non-linear solver.

Another goal will be the implementation of uCRM-13.5 wing structural model within the optimization framework in order to apply multifidelity to unconstrained, and then unconstrained optimization problems.

## ACKNOWLEDGEMENTS

The authors would like to thank FONISEN and European project U-HARWARD for funding this research project and ONERA strong partnership in the development of MF-EGO/MF-SEGO (N. Bartoli, T. Lefevbre, R. Lafage, in particular). We also want to thanks Joan Mas Colomer for his constant help.

## REFERENCES

- [1] G. K. W. Kenway and J. R. R. A. Martins. Multipoint High-Fidelity Aerostructural Optimization of a Transport Aircraft Configuration. *Journal of Aircraft*, 51(1):144–160, Jan. 2014. doi:10.2514/1.C032150. URL <https://arc-aiaa-org.rev-doc.isae.fr/doi/10.2514/1.C032150>. Publisher: American Institute of Aeronautics and Astronautics.
- [2] M. C. Kennedy and A. O’Hagan. Predicting the output from a complex computer code when fast approximations are available. *Biometrika*, 87(1):1–13, 2000. ISSN 00063444.
- [3] D. R. Jones. A taxonomy of global optimization methods based on response surfaces. *Journal of Global Optimization*, 21(4):345–383, Dec 2001.
- [4] D. R. Jones, M. Schonlau, and W. J. Welch. Efficient global optimization of expensive black-box functions. *Journal of Global Optimization*, 13(4):455–492, Dec 1998.
- [5] N. Bartoli, I. Kurek, R. Lafage, T. Lefebvre, R. Priem, M. A. Bouhrel, J. Morlier, V. Stiliz, and R. Regis. Improvement of efficient global optimization with mixture of experts: methodology developments and preliminary results in aircraft wing design. 06 2016.
- [6] N. Bartoli, M. Meliani, J. Morlier, T. Lefebvre, M.-A. Bouhrel, and J. Martins. *Multifidelity efficient global optimization: Methodology and application to airfoil shape design*. 2019. doi:10.2514/6.2019-3236. URL <https://arc.aiaa.org/doi/abs/10.2514/6.2019-3236>.
- [7] J. Mas-Colomer. *Aeroelastic Similarity of a Flight Demonstrator via Multidisciplinary Optimization*. PhD thesis, 12 2018.
- [8] J. M. Colomer. Aerostructure package, 2019. URL <https://github.com/mid2SUPAERO/aerostructures>.
- [9] G. R. Jiménez and J. M. J. Mas Colomer. Multifidelity aeroelastic optimization with application to a bwb. *AIAA Aviation*, 2021.
- [10] openMDAO. Openmdao source docs, 2016. URL [http://openmdao.org/twodocs/versions/2.2.0/\\_srcdocs/index.html](http://openmdao.org/twodocs/versions/2.2.0/_srcdocs/index.html).
- [11] T. Scholcz. Multi-fidelity methods for fluid-structure interaction and uncertainty quantification. 09 2015.
- [12] Z. Guo, L. Song, C. Park, J. Li, and R. T. Haftka. Analysis of dataset selection for multi-fidelity surrogates for a turbine problem. *Structural and Multidisciplinary Optimization*, 57(6):2127–2142, Jun 2018. ISSN 1615-1488. doi:10.1007/s00158-018-2001-8. URL <https://doi.org/10.1007/s00158-018-2001-8>.
- [13] G. Fernandez, C. Park, N. Kim, and R. Haftka. Issues in deciding whether to use multifidelity surrogates. *AIAA Journal*, pages 1–16, 03 2019. doi:10.2514/1.J057750.

- [14] Boeing. *A502I User's Guide-PAN AIR Technology Program for Solving Potential Flow about Arbitrary Configurations*. 02 1992.
- [15] NASA. *The Nastran User's Manual*. 12 1980.
- [16] NASA. Nasa common research model, 2017. URL <https://commonresearchmodel.larc.nasa.gov/>.
- [17] M. Pástor, M. Binda, and T. Harčarik. Modal assurance criterion. *Procedia Engineering*, 48:543–548, 12 2012. doi:10.1016/j.proeng.2012.09.551.
- [18] T. R. Brooks, G. K. Kenway, and J. R. R. A. Martins. Undelected Common Research Model (uCRM): An Aerostructural Model for the Study of High Aspect Ratio Transport Aircraft Wings. In *35th AIAA Applied Aerodynamics Conference*. American Institute of Aeronautics and Astronautics. doi:10.2514/6.2017-4456.
- [19] A. C. Gray and J. Martins. Geometrically Nonlinear High-fidelity Aerostructural Optimization for Highly Flexible Wings. In *AIAA Scitech 2021 Forum*, AIAA SciTech Forum. American Institute of Aeronautics and Astronautics, Jan. 2021. doi:10.2514/6.2021-0283.